Acta Oceanol. Sin., 2017, Vol. 36, No. 3, P. 60–71
DOI: 10.1007/s13131-017-0977-3
http://www.hyxb.org.cn
E-mail: hyxbe@263.net

Temporal and spatial variability of the carbon cycle in the east of China's seas: a three-dimensional physical-biogeochemical modeling study

JI Xuanliang[1, 2], LIU Guimei[1, 2*], GAO Shan[1, 2], WANG Hui[1, 2], ZHANG Miaoyin[1, 2]

[1] National Marine Environmental Forecasting Center, State Oceanic Administration, Beijing 100081, China

[2] Key Laboratory of Research on Marine Hazards Forecasting, National Marine Environmental Forecasting Center, State Oceanic Administration, Beijing 100081, China

Received 7 December 2015; accepted 31 May 2016

Abstract

In the east of China's seas, there is a wide range of the continental shelf. The nutrient cycle and the carbon cycle in the east of China's seas exhibit a strong variability on seasonal to decadal time scales. On the basis of a regional ocean modeling system (ROMS), a three dimensional physical-biogeochemical model including the carbon cycle with the resolution (1/12)°×(1/12)° is established to investigate the physical variations, ecosystem responses and carbon cycle consequences in the east of China's seas. The ROMS-Nutrient Phytoplankton Zooplankton Detritus (NPZD) model is driven by daily air-sea fluxes (wind stress, long wave radiation, short wave radiation, sensible heat and latent heat, freshwater fluxes) that derived from the National Centers for Environmental Prediction (NCEP) reanalysis2 from 1982 to 2005. The coupled model is capable of reproducing the observed seasonal variation characteristics over the same period in the East China Sea. The integrated air-sea CO_2 flux over the entire east of China's seas reveals a strong seasonal cycle, functioning as a source of CO_2 to the atmosphere from June to October, while serving as a sink of CO_2 to the atmosphere in the other months. The 24 a mean value of air-sea CO_2 flux over the entire east of China's seas is about 1.06 mol/(m^2·a), which is equivalent to a regional total of 3.22 Mt/a, indicating that in the east of China's seas there is a sink of CO_2 to the atmosphere. The partial pressure of carbon dioxide in sea water in the east of China's seas has an increasing rate of 1.15 μatm/a (1μtm/a=0.101 325 Pa), but pH in sea water has an opposite tendency, which decreases with a rate of 0.001 3 a^{-1} from 1982 to 2005. Biological activity is a dominant factor that controls the p_{CO_2air} in the east of China's seas, and followed by a temperature. The inverse relationship between the interannual variability of air-sea CO_2 flux averaged from the domain area and Niño3 SST Index indicates that the carbon cycle in the east of China's seas has a high correlation with El Niño-Southern Oscillation (ENSO).

Key words: the east of China's seas, physical-biogeochemical model, partial pressure of carbon dioxide in sea water, air-sea CO_2 flux

Citation: Ji Xuanliang, Liu Guimei, Gao Shan, Wang Hui, Zhang Miaoyin. 2017. Temporal and spatial variability of the carbon cycle in the east of China's seas: a three-dimensional physical-biogeochemical modeling study. Acta Oceanologica Sinica, 36(3): 60–71, doi: 10.1007/s13131-017-0977-3

1 Introduction

Over the past decade, scientists have focused on the study of an air-sea CO_2 flux over the continental shelf sea. As a linkage between the land and the vast ocean, the continental shelf sea is affected by human activities, as well as the physical, biological and chemical processes. On one hand, under the influences of the biological activities, the partial pressure of carbon dioxide in sea water in surface waters declined due to carbonate absorption by phytoplankton; on the other hand, with the supply of carbonate from river water and deep sea water, the partial pressure of carbon dioxide in sea water would increase markedly (Tseng et al., 2011). Considering the two factors exist simultaneously while resist with each other, the problems about the air-sea CO_2 flux in the continental shelf sea become more and more complex. Some results show that the continental shelf sea is the source of CO_2 to the atmosphere (Naqvi et al., 2005); however, some results suggest that it is a sink of CO_2 to the atmosphere, and the flux ranges from 0.2 to 1 Gt/a (Tsunogai et al., 1999). According to the study in the North Sea, Bozec et al. (2005) find that the intense biological activities make the northern North Sea serves as a sink of CO_2 to the atmosphere, and the high concentration of inorganic carbon supplement from river make the southern North Sea serves as a source of CO_2 to the atmosphere. Meanwhile, Cai et al. (2006) show that the continental shelves can be either a large

Foundation item: The National Key Research and Development Program of China under contract No. 2016YFC1401605; the Strategic Priority Research Program of the Chinese Academy of Sciences under contract No. XDA 1102010403; the National Natural Science Foundation of China under contract Nos 41222038, 41206023 and 41076011; the Public Science and Technology Research Funds projects of Ocean of China under contract No. 201205018; the National Key Research and Development Program of China under contract No. 2016YFC1401605; the Guangdong Provincial Key Laboratory of Fishery Ecology and Environment under contract No. LFE-2015-3.

*Corresponding author, E-mail: liugm@nmefc.gov.cn

sink or a source for atmospheric CO_2, and they suggested that those shelves can generally be a sink for atmospheric CO_2 at mid to high latitudes and a source of CO_2 at low latitudes. However, previous fieldwork and syntheses have only focused on a limited number of locations and the role of the vast majority of the shelves in the carbon budget remains unclear. Hence, as one of the biggest marginal seas in the world, understanding of the carbon cycle in the east of China's seas (21°–41°N, 114°–133°E) (Fig. 1) helps us to quantify the role of the marginal seas in the global carbon cycle.

Because of the complex currents, monsoon, nutrients discharge, atmospheric deposition, bottom sediments and so on, the east of China's seas is with characteristics of high nutrient level, rich fishery resources, plenty of planktons and high productivity. Meanwhile, under the physical, biological and chemical processes, the carbon cycle process in the east of China's seas is divided into solubility pump, biology pump and carbonate pump. Considering the importance of the carbon cycle in the east of China's seas, not a few scholars have developed the study on carbon budget in the east of China's seas. Zhang and Zhang (2008) pointed out that the Bohai Sea performs as a source of CO_2 in summer, as a result of the nutrients discharge from river. Xue et al. (2011) pointed out that the entire South Yellow Sea (SYS) is a net source of atmospheric CO_2 in summer, winter and fall, whereas it is a net sink in spring; and the SYS is a net source on an annual scale, releasing approximately 7.38 Mt to the atmosphere annually. Compared with the Bohai Sea and the Yellow Sea, the study on the carbon cycle in the ECS is relatively intact. Tsunogai et al. (1997, 1999) reported a net air-sea CO_2 flux of –2.9 mol/(m^2·a) extrapolated from the relationships between the partial pressure of carbon dioxide in sea water and other parameters obtained from 14 stations along the PN line (from 31.4°N, 123°E to 27.5°N, 128.4°E). Wang et al. (2000) surveyed the carbonate system in spring and summer in the east part of the ECS and estimate a net air-sea CO_2 flux of –1.2 to –2.8 mol/(m^2·a). However, Shim et al. (2007) obtained a relatively smaller value of the net air-sea CO_2 flux, which is –0.87 mol/(m^2·a). Although the factors that regulate the air-sea CO_2 flux have been regularly explored by previous observers, due to the lack of long-term data across most of the east of China's seas, the temporal and spatial variations of the carbon cycle in the east of China's seas have not yet been elucidated, and the processes controlling the partial pressure of carbon dioxide in sea water variation are not fully understood.

A modeling approach has been taken to assess the relative importance of the interactions between the various processes (physical, biological, chemical processes) and the carbon cycle. A number of diagnostic and 3-D ocean modeling studies are used to estimate the air-sea CO_2 flux in the South China Sea and the tropical Pacific, and the results from these models show a good agreement with the observations (Wang et al., 2006; Chai et al., 2009; Lu et al., 2012). However, very few previous modeling studies have applied their marine ecosystem models in the east of China's seas. In this study, a physical and biogeochemical model, incorporating the oceanic carbon cycling and air-sea CO_2 exchange, is used to examine seasonal and interannual variations of the air-sea CO_2 flux in the east of China's seas. The model framework and experimental design are explained in the next section. The modeled temperature, salinity, NO_3, dissolved oxygen (DO) and total alkalinity (TA) are compared with observation data in Section 3. The predominant factors controlling the the partial pressure of carbon dioxide in sea water and the air-sea CO_2 flux in the east of China's seas are discussed in Section 4. Section 5 summarizes the results obtained in this study.

2 Methods and data

2.1 *Physical model*

The physical model for this study is based on a regional ocean model system (ROMS), which represents an evolution in the family of terrain-following vertical-coordinate models. It solves the primitive equations with hydrostatic and Boussinesq approximations. The ROMS contains innovative algorithms for advection, pressure-gradient force, free-surface variations, and K-profile vertical-mixing parameterizations for surface and bottom boundary layers (Large et al., 1994; Shchepetkin and McWilliams, 2003). For this modeling study, we configured an ROMS circulation

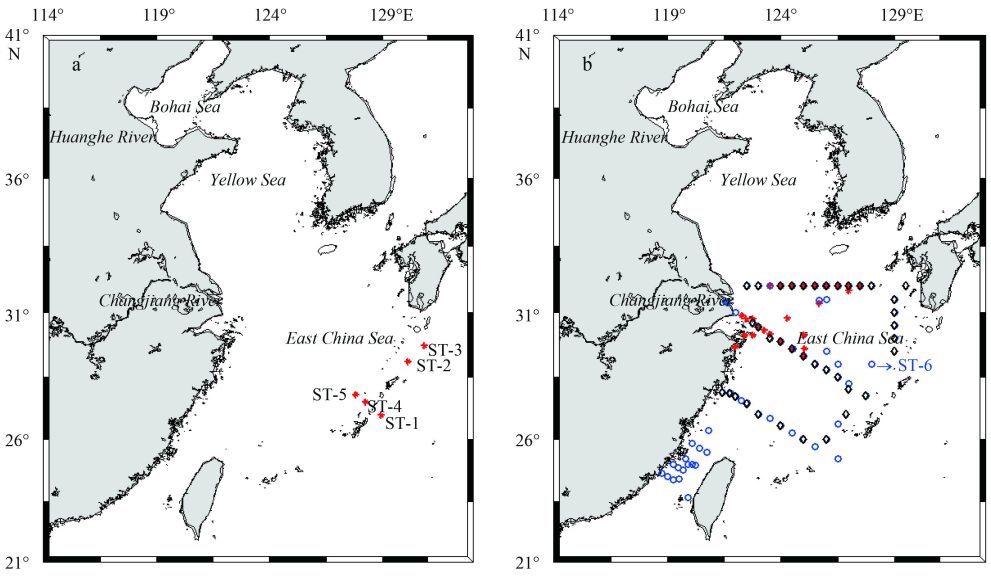

Fig. 1. Study area of China's coastal seas. a. Observation data derived from Japan survey profiles (1993/10); and b. observation data derived from JGOFS-1 (1993/10, red star), JGOFS-2 (1994/04, blue circle) and JGOFS-3 (1994/10, black diamond). The observation data includes temperature, salinity, dissolved oxygen, NO_3, total alkalinity.

model for the northwestern Pacific (NWP, 3°–52°N, 98°–158°E) with (1/12)°×(1/12)° of horizontal resolution, 5 d of temporal resolution and 22 sigma levels (Fig. 2).

2.1.1 *Topography data*

The topography data are derived from General Bathymetric Chart of the Oceans (GEBCO) (https://www.bodc.ac.uk/data/online_delivery/gebco/), which is a global 30 arc-second grid largely generated by combining quality-controlled ship depth soundings with interpolation between sounding points guided by satellite-derived gravity data. To insure the stability of the model, the bathymetry is smoothed and calibrated by a tidal range appropriately. Meanwhile, the water depth less than 15 m is set as 15 m, and the maximum bathymetry is set as 5 000 m (Fig. 2).

2.1.2 *Boundary data*

Considering the influence of inflow and outflow in the boundary, we set the southern, eastern and northern boundaries as an open boundary (Blumberg and Kantha, 1985). The lateral boundary conditions used for the physical model are FSCHAPMAN, M2FLATHER, M3RADIATION, M3NUDGING, TRADIATION and TNUDGING. Under a climatology run, the data for temperature, salinity, zeta, u, v, ubar and vbar in the three open boundaries is derived from simple ocean data assimilation (SODA) climatological data (http://soda.tamu.edu/assim/SODA_2.2.4/). While under a high-forcing run, the lateral boundary data are from SODA monthly data.

2.1.3 *Forcing data*

The model is forced by a wind stress, heat fluxes (long wave radiation, short wave radiation, sensible heat and latent heat) and freshwater fluxes (evaporation and precipitation). As data source of the forcing filed, two kinds of data are used. One is the climatological data from comprehensive oceanic and atmosphere data sets (COADS) (http://iridl.ldeo.columbia.edu/SOURCES/.COADS/)). The other is National Centers for Environmental Prediction AMIP-II Reanalysis II daily data (http://www.esrl.noaa.gov/psd/data/gridded/data.ncep.reanalysis2.html).

2.1.4 *Initialization data*

The temperature and the salinity in the initial field are derived from the World Ocean Atlas (WOA2009) data in December with a spatial resolution of 1°×1° and 24 vertical layers (http://www.nodc.noaa.gov/OC5/WOA09/netcdf_data.html). Meanwhile, *u*, *v* and zeta are set as 0.

2.2 *Biology model*

The biogeochemical model is linked to the physical model with the same spatial and temporal resolutions. It is a representation of the pelagic nitrogen cycle and contains 12 compartments, including phytoplankton, chlorophyll *a* (Chl *a*), NO_3, NH_4, zooplankton, large detritus nitrogen, small detritus nitrogen, large detritus carbon, small detritus carbon, total inorganic carbon (TIC), TA, and DO (Fig. 3). Considering the biological characteristics in the east of China's seas, we mainly focus on the modifications of the biological process (Ji et al., 2015), and optimized controlling equations and biological parameters have been shown in Ji et al. (2015). The other details of the model formulations were described by Fennel et al. (2006).

2.2.1 *Air-sea CO_2 flux formulation*

The partial pressure of carbon dioxide in sea water is calculated from temperature, salinity, TIC and TA. As shown in Fig. 3, both TIC and TA are affected by the biology process and the physical process. The formulation of the partial pressure of carbon dioxide in sea water is as follows:

$$p_{\mathrm{CO_2sea}} = \frac{c_{\mathrm{tic}}}{K_{\mathrm{s}}}\left(\frac{c^2(\mathrm{H}^+)}{c^2(\mathrm{H}^+) + K_1 \times c(\mathrm{H}^+) + K_1 \times K_2}\right), \quad (1)$$

where $c\,(H^+)$ is the concentration of hydrogen ion, K_1 is the first dissociation constant of carboinic acid, K_2 is the second dissociation constant (Millero, 1995), and K_s is solubility coefficient of CO_2 in the sea water (Weiss and Price, 1980).

The air-sea CO_2 flux is calculated with

$$F_{\mathrm{CO_2}} = k \times K_{\mathrm{s}} \times \Delta p(\mathrm{CO_2}), \quad (2)$$

where k is the gas exchange rate; $\Delta p\,(CO_2)$ is the difference between the partial pressure of carbon dioxide in sea water and the partial pressure of carbon dioxide in air.

The gas exchange rate k is calculated through a wind speed under steady wind conditions according to Wanninkhof (1992):

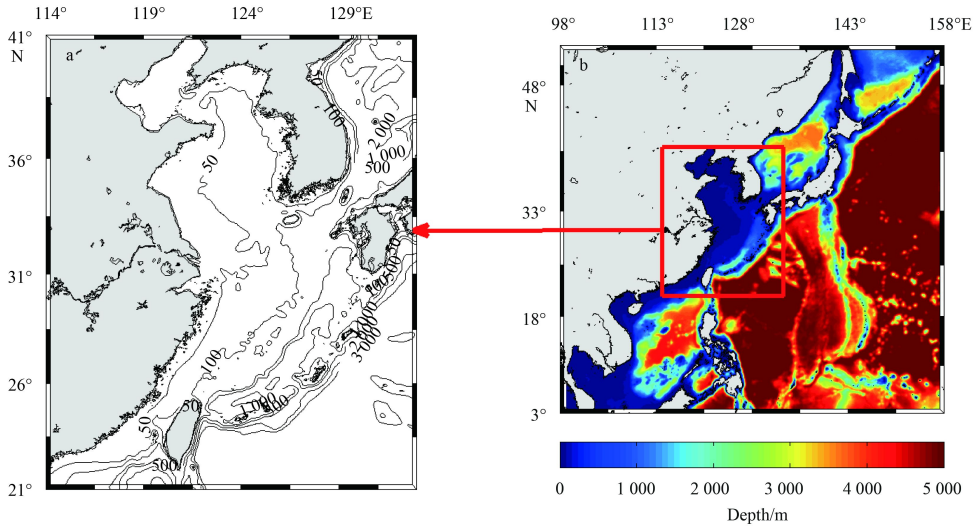

Fig. 2. China's coastal seas (a, study area) with isobaths (m) and bathymetry of the northwestern Pacific Ocean (b, modeled area).

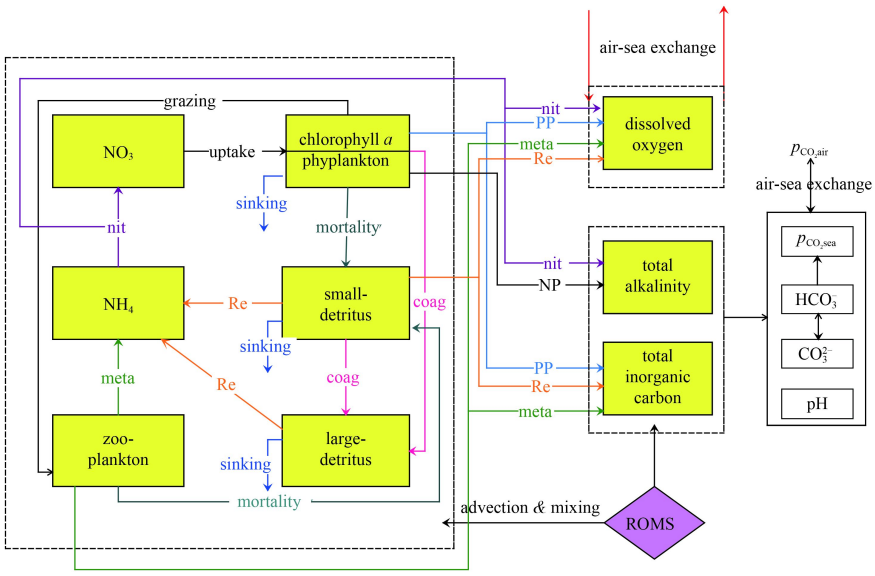

Fig. 3. A schematic of the nitrogen-based biogeochemical model. nit represents nitrification, PP primary production, meta metabolism, NP new production, and Re remineralization; Coa: Coagulation.

$$k = 0.31 \times u^2 \times \left(\frac{S_c}{660}\right)^{-\frac{1}{2}}, \quad (3)$$

where u is the wind speed at 10 m above sea level calculated from the wind stress; and S_c is the Schmidt number for CO_2 which is a function of the SST (Wanninkhof, 1992), as follows:

$$S_c = a_1 - T \times [a_2 - \mathrm{T} \times (a_3 - \mathrm{T} \times a_4)], \quad (4)$$

where T is the temperature (°C); a_1, a_2, a_3 and a_4 are constants with the value of 2 073.1, 125.62, 3.627 6 and 0.043 219.

2.2.2 *Biology model data*

NO_3, TA, TIC and DO are initialized from the World Ocean Atlas (WOA2009) in December (http://www.nodc.noaa.gov/OC5/WOA09/netcdf_data.html). The chorophyll *a* in the initial field is derived from SeaWiFS (http://oceandata.sci.gsfc.nasa.gov.SeaWiFS) using a vertical interpolation formula (Morel and Berthon, 1989) as follows. Phytoplankton and zooplankton in the initial field are calculated from Chl *a* by a rate of 0.5. Four kinds of detritus are calculated from phytoplankton by a ratio of 0.35 (Gruber et al., 2006). NH_4 is set as 1 mmol/m^3.

In the lateral boundary, the data for NO_3, TA, TIC and DO are from WOA09, for Chl *a* is from SeaWiFS, and for the other variables are calculated from Chl *a* concentration based on a correlation coefficient. The calculation function for the vertical Chl *a* concentration is used from Morel and Berthon (1989), which is calculated as follows:

$$C_a = C_{pz} \times \left\{C_{a,s} + C_{a,\max} \times \exp\left[-\left((\zeta - \zeta_{\max})/\Delta\zeta\right)^2\right]\right\}, \quad (5)$$

where $C_{a,\max}$ is the maximum value of Chl *a* concentration; $C_{a,s}$ is the surface concentration of Chl *a*; ζ=Z/Z_{pz}, Z is the seawater depth, Z_{pz} is the thickness of a photic zone.

River discharges are also set up with source of nutrients (NO_3 and NH_4) (Zhang, 1996; Duan and Zhang, 1999; Zhang et al., 2010), which includes the four rivers: Huanghe River, Changjiang River, Zhujiang River and Mekong River.

2.2.3 *Spin-up*

When running the model, the internal model time step is set as 600 s, and the external model time step is 30 s. The ROMS-NPZD model is first spun up for 10 a using the COADS climatological data to reach a statistical equilibrium. After the 10 a spin up, the model is integrated for the period of 1979–2005 forced with NCEP reanalysis2 daily data, and the modeled data from 1982–2005 is selected to study.

2.3 *Observational data*

Observation data in the ECS from 1993 to 1994 (Fig. 1) are used to compare with the modeled results. Aside from the measurements of the temperature and the salinity, discrete water samples were collected for determination of DO, TA and NO_3. The station data at Sites 1, 2, 3, 4, 5 (ST-1, ST-2, ST-3, ST-4, ST-5) shown in Fig. 1a are from the survey cruises by Japan scientists from September to October in 1993. The observation data shown in Fig. 1b are derived from the survey cruises through the joint global ocean flux study in October 1993(JGOFS-1), April 1994 (JGOFS-2) and October 1994 (JGOFS-3), which is described in detail by Qiao et al. (2005). The JGOFS is an international and multi disciplinary programme with participants from more than 20 nations. Nine cruises of "margin flux in the East China Sea" project in East China Sea were carried out over the period from October 1993 to July 1998 (http://ijgofs.whoi.edu/). The ship of *Venus* is used for the JGOFS-1 survey cruise in October 1993. The ship of *Kexue 1* is used for the JGOFS-2 survey cruise in April 1993, and *Dongfanghong 2* is used for the JGOFS-3 survey cruise in Ocotber 1994. During the survey cruises, temperature and salinity were measured in the field with a conductivity, temperature and depth (CTD) detector. DO was measured using an iodine stoichiometry titration method. Nitrate was measured using a zinc cadmium reduction method.

3 Results

3.1 *Model validation*

The variation of the partial pressure of carbon dioxide in sea water is simultaneously affected or controlled by multiple factors.

First, we evaluated the model performance by directly comparing the model results with the observations. Figure 4 shows the modeled temperature, salinity, DO, NO_3 and TA profiles above 1 000 and 100 m depth of water in April 1994 (Fig. 4b) and above 1 000 and 200 m depth of water in October 1993 (Fig. 4a), respectively. The corresponding profiles of the observations are also shown in Fig. 4. Generally, the modeled results have good agreement with observation results. As shown in Fig. 4, the mean errors between the modeled temperature and the observed data above 100 m in April and above 200 m in October are 0.60°C and 0.63°C, respectively, which means that high resolution modeled results could capture the distribution characteristics of thermocline. Meanwhile, the value of ROMS-NPZD modeled salinity falls within the range of the observations. The mean errors of the salinity between the observed and modeled salinities in April and October are 0.20 and 0.12, respectively. However, the largest deviation for the salinity reaches at 0.8 on the surface in April 1994 (Fig. 4b). The main reason for this deviation in surface is the air fluxes, such as precipitation and evaporation. But the deviation is small in other depths. Hence, the vertical variability of the modeled temperature and salinity exhibits similar features to the observations. In addition, the high resolution model reproduces the observed DO, NO_3 and TA concentration profiles reasonably well, but the predicted NO_3 concentrations are higher on the surface than the observations in October which may be resulted from the higher upward NO_3 flux from vertical upwelling (Fig. 4). The deviation range for TA at the upper 200 m level is from 5 to 35 mmol/m^3. The reason for this deviation may be the biological model cannot perform the carbon transport well. But the deviation is less than the modeled results from Liu et al. (2009). Overall, the general good agreement between the model and the observations indicates that the model captures the characterized response to the internal biological processes and external forcing reasonably well. The validated model provides a solid basis for the mechanism analysis of the carbon cycle.

For further validation, Fig. 5 shows the linear regressions of the temperature, the salinity, DO and NO_3 between the modeled results and the observations from Japan and JGOFS-2 shown in Fig. 1. We only compare the observations and the model results for the upper 1 000 m. The linear regression slopes for the temperature, the salinity, DO and NO_3 concentrations are 0.94, 0.94, 0.89 and 0.95, respectively. Meanwhile, the high R-square values are obtained for all four variables, 0.95 for the temperature, 0.91 for the salinity, 0.88 for DO, and 0.95 for NO_3, which indicates that the model is capable of reproducing the absolute values for both the physical variables and biological variables.

As shown in Fig. 4, the profile comparison between the modeled results and the observations is not good enough in the upper 100 m, especially the NO_3. However, the biology activity in the euphotic zone has an important influence on the carbon cycle. Hence, the observation data collected by the ship in October 1993, April 1994 and October 1994 are used. There are 26 stations for the JGOFS-1, 68 stations for the JGOFS-2 and 38 stations for the JGOFS-3 (Fig. 1b). Meanwhile, the numbers of effective sample are listed in Table 1. On the basis of these data, the ME and MAE of the temperature, the salinity, DO, NO_3 and Chl *a* between the observations and the modeled results in the upper 100 m are analyzed.

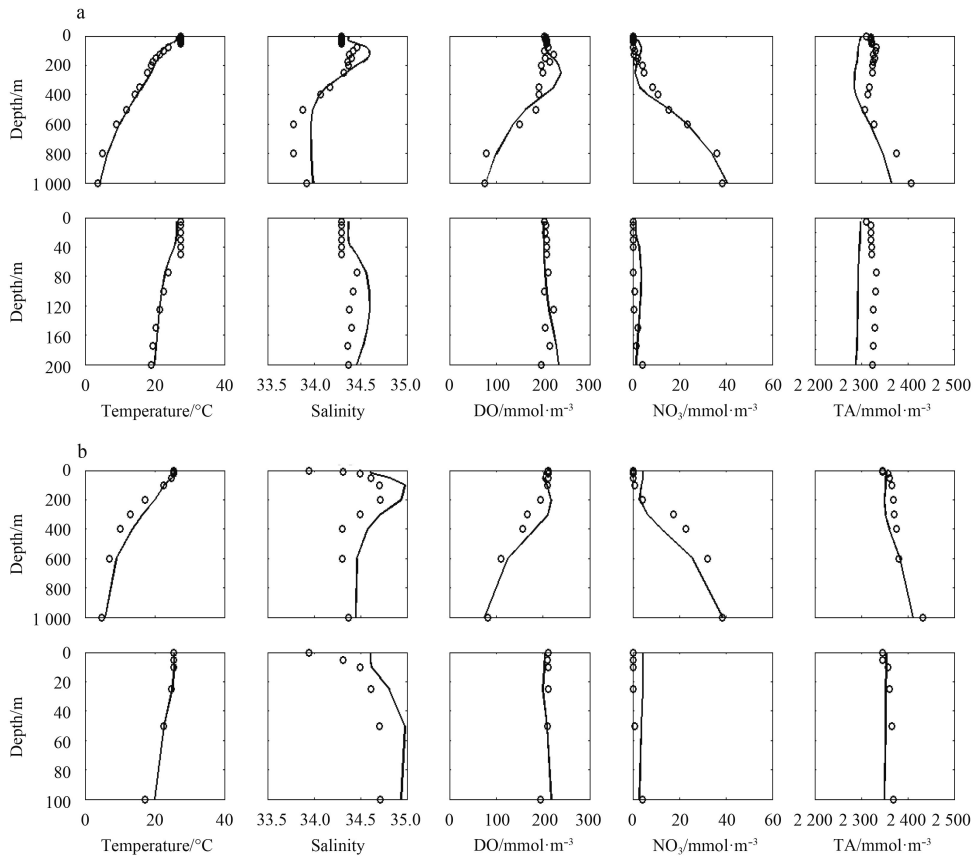

Fig. 4. Comparison between the observed (open circle) and the modeled (solid line) profiles of the whole water column and the top 200 m in October 1993 (a, ST-1) and the whole water column and the top 100 m in April 1994 (b, ST-6), respectively.

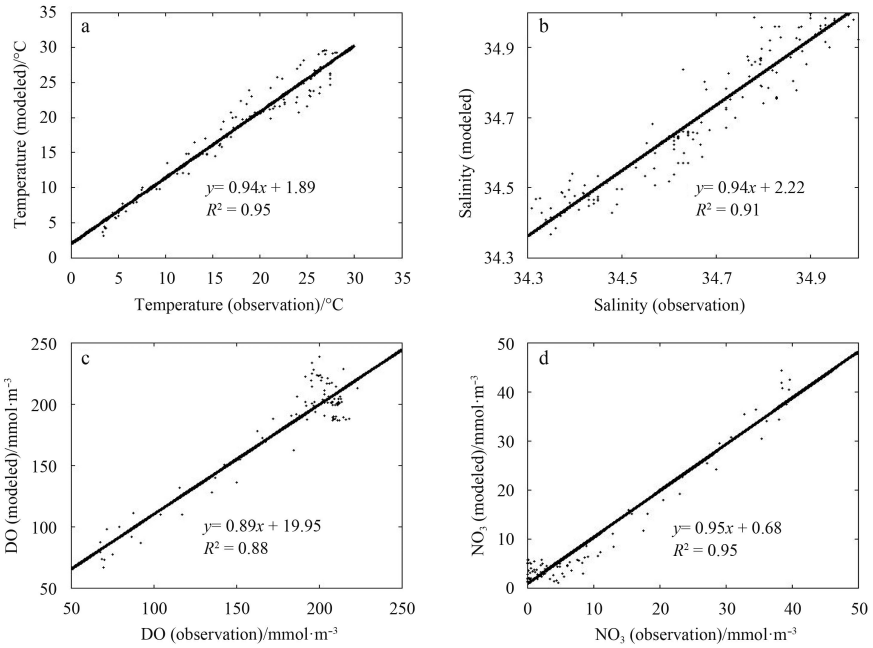

Fig. 5. ROMS-NPZD model of temperature (a), salinity (b), DO (c) and NO_3 (d) vs. observation data from November 1993 to April 1994.

For the upper 100 m depth, the averaged ME value is –0.19°C, 0.28, –7.51 mmol/m³, 1.81 mmol/m³ and 0.06 mg/m³ for the temperature, salinity, DO, NO_3 and Chl *a*, respectively. According to ME value shown in Figs 6a–e), the concentration of the modeled salinity, NO_3 and Chl *a* is higher than that from the observations in the upper 100 m, while the concentration of the modeled DO is lower than that of the observed DO. For the temperature, the modeled results are higher than observed results from 0 to 30 m, while lower in 50 and 100 m.

Table 1. Numbers of effective sample

Depth/m	Temperature	Salinity	DO	NO_3	Chl *a*
0	96	108	93	65	29
10	77	77	82	57	27
20	93	98	82	60	29
30	45	57	46	45	21
50	21	41	30	25	18
100	11	23	18	23	0

Meanwhile, for the upper 100 m depth, the averaged MAE value is 1.37°C, 0.50, 12.11 mmol/m³, 2.35 mmol/m³ and 0.29 mg/m³ for the temperature, salinity, DO, NO_3 and Chl *a*. As shown in Fig. 6f, the maximum MAE value of the temperature is

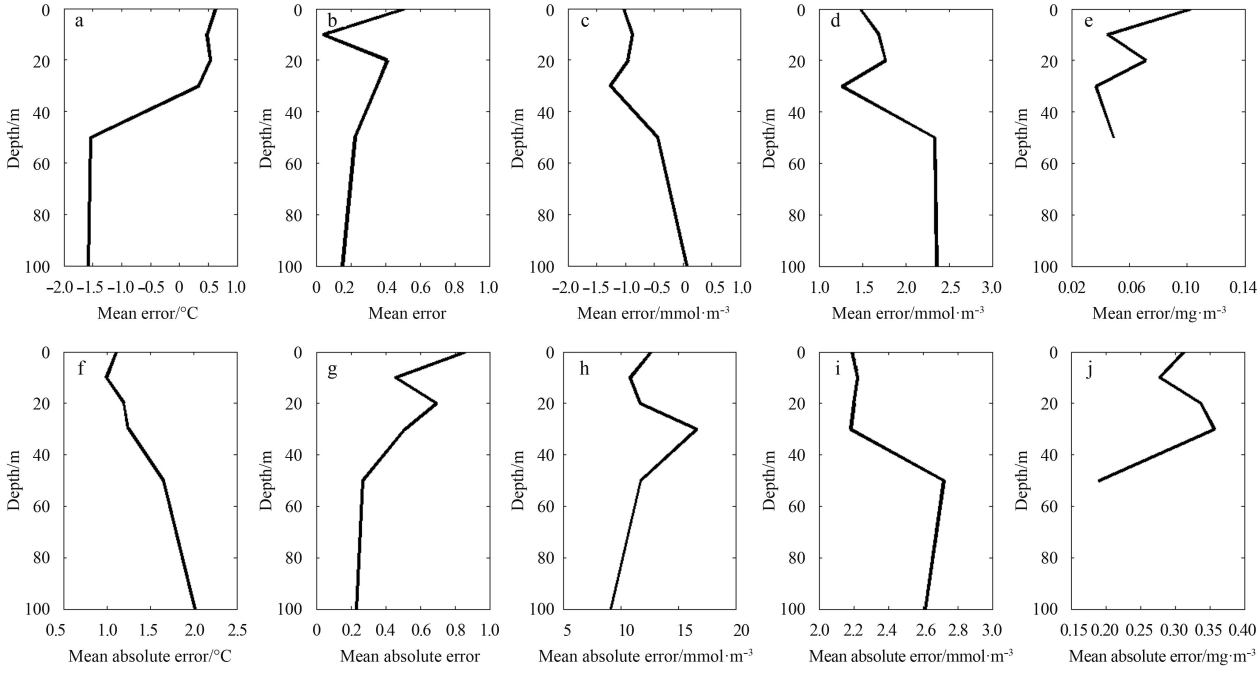

Fig. 6. Mean error (a, b, c, d and e) and mean absolute error (f, g, h, i and j) of the temperature, salinity, DO, NO_3 and Chl *a*, respectively.

2.01°C at 100 m depth, and the minimum value is 0.99°C at 10 m depth. For the salinity shown in Fig. 6g, the maximum MAE value is 0.86 on the surface, and the minimum value is 0.23 at 100 m depth, which shows a decreasing trend with depth. However, for DO (Fig. 6h), the maximum MAE value is 16.61 mmol/m^3 at 30 m depth, and the minimum value is 9.14 mmol/m^3 at 100 m depth. For NO_3 shown in Fig. 6i, the maximum MAE value is 2.72 mmol/m^3 at 50 m depth, and the MAE values at other depth are higher than 2 mmol/m^3. The possible reason for this difference between the modeled NO_3 and the observed NO_3 is that the concentration of NO_3 in the ECS region in initial field derived from WOA09 is higher than the observation data; meanwhile, the concentration of NO_3 added in Changjiang River is another reason. Owing to the higher concentration of NO_3 in the model, the concentration of Chl *a* from the model is also higher than that from the observation data (Fig. 6j). The maximum MAE is 0.36 mmol/m^3 at 30 m depth.

The main purpose of this paper is to study the variation characteristics of the partial pressure of carbon dioxide in sea water and the air-sea CO_2 flux. The conclusion that biological activity has an obvious influence on the distribution of the partial pressure of carbon dioxide in sea water and the air-sea CO_2 flux has been proposed by Chai et al. (2009). Hence, in order to validate the model's performance on the biological activity, we undertake a comparison experiment between the modeled Chl *a* and the observed Chl *a* from the SeaWiFS from 1997 to 2005, whose results are shown in Fig. 7. On the basis of the satellite data (Fig. 7, blue line), the concentration of Chl *a* has a double-peak structure in 1 a, the maximum value is in spring and the second-maximum value is in autumn. The modeled Chl *a* has the same seasonal variation characteristic, and the monthly variation from the model is similar to the results from Hu et al. (2004), Liu and Yin (2007) and Zheng et al. (2012). The concentration of the modeled Chl *a* is less than that of the observed Chl *a*, especially in winter. The concentration of Chl *a* in the south of the Yellow Sea in winter is in a range of 0.3–0.6 mg/m^3 simulated by Hu et al. (2004) using POM model, and is in a range of 0.2-0.6 mg/m^3 in the Bohai Sea in winter simulated by Liu and Yin (2007). Hence, the concentration of Chl *a* from satellite in winter is a bit higher than that from *in situ* data. The main reason for this deviation is the uncertainty of the satellite data, especially in the near shore region. The calculation method for the concentration of Chl *a* from the SeaWiFS is based on Case I water (Wang and Shi, 2005; Wang et al., 2007). However the property of the study area belongs to Case II water, the ocean color would be affected by the concentration of Chl *a*, suspended matter and yellow substance. Hence, the absolute concentration of Chl *a* would be overestimated by the calculation method of Case I water.

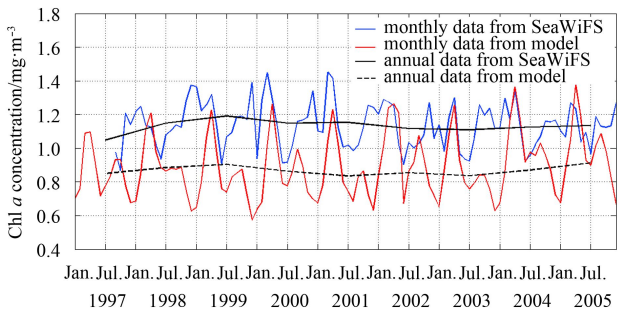

Fig. 7. Comparison between the Chl *a* concentration from the model and the satellite.

3.2 *Seasonal variation of partial pressure of carbon dioxide in sea water*

The modeled climatological partial pressure of carbon dioxide in sea water shows strong seasonal variations (Fig. 8). In February, from north to south, the partial pressure of carbon dioxide in sea water increases with the decrease of latitude from 250 μatm in the north to 370 μatm in the south (Fig. 8a). The areas with being less than 250 μatm value are located in the Bohai Sea, Yellow Sea and the northern ECS, while areas with higher value (>350 μatm) are located in the southern ECS. Owing to the warm water and high nutrient concentration from the Kuroshio, the partial pressure of carbon dioxide in sea water is higher than 350 μatm in the path of the Kuroshio, especially in the east of Taiwan Province. In May, as shown in Fig. 8b, the partial pressure of carbon dioxide in sea water has a prominent increase with a maximum increasing gradient of 250 μatm. In August (Fig. 8c), the partial pressure of carbon dioxide in sea water reaches the peak value comparing with the other three months in the east of China's seas. Because of the nutrients supplement from the Changjiang Diluted Water, a higher value (~600 μatm) appears in the Changjiang Estuary compared with the adjacent ocean areas. Meanwhile, under the function of upwelling, the partial pressure of carbon dioxide in sea water in the west of the Yellow Sea is higher than that in the center. Since the lowest partial pressure of carbon dioxide in sea water in August is above 400 μatm, which is still higher than that of the atmosphere, the CO_2 flux is from the sea to the air for the entire region of the east of China's seas. In November (Fig. 8d), the value of the partial pressure of carbon di-

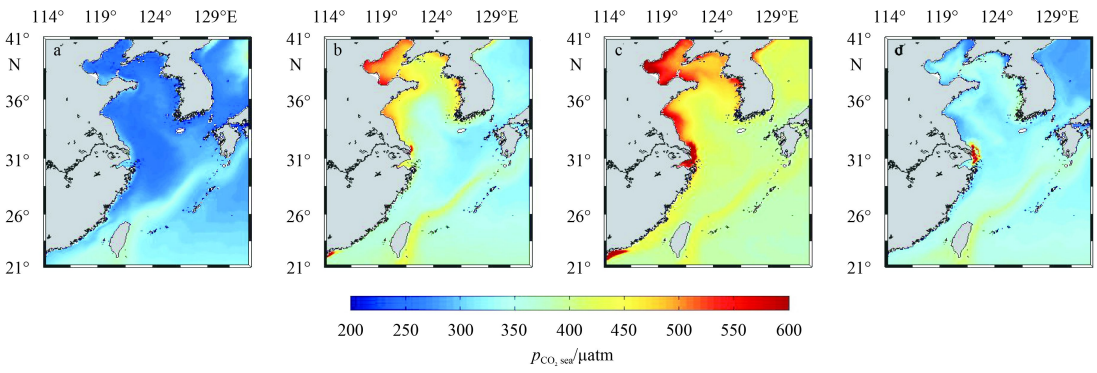

Fig. 8. The modeled surface climatological distributions of the partial pressure of carbon dioxide in sea water averaged from 1982 to 2005 in the east of China's seas. a. February, b. May, c. August, and d. November.

oxide in sea water has an obvious decrease, but it is still higher than that in February. The partial pressure of carbon dioxide in sea water is lower than 360 μatm in most areas where it performs as the sink of CO_2 to the atmosphere. Overall, the climatological monthly spatial partial pressure of carbon dioxide in sea water distribution in the east of China's seas varies geographically.

3.3 *Seasonal and interannual variation of air-sea CO_2 flux*

The air-sea CO_2 flux is averaged over the entire east of China's seas and evaluated from 1982 to 2005 (Fig. 9). As shown in Fig. 9, the air-sea CO_2 flux presents a prominent seasonal variation. The east of China's seas domain-averaged monthly CO_2 flux from air-sea varies from –1.41 to 4.38 mol/(m²·a) with the lowest value in summer and highest value in winter. The east of China's seas acts as a source of CO_2 to the atmosphere from June to October. The monthly minimum value of the air-sea CO_2 flux in August ranges from –2.09 to –0.44 mol/(m²·a), with the minimum value in August 1997 and the largest value in 1988, which indicates the positive SST anomaly favors the increase of the partial pressure of carbon dioxide in sea water in surface water and reduction of the CO_2 flux. In other months, the east of China's seas serves as the sink of CO_2 to the atmosphere, which reaches the maximum value in January from 3.14 to 5.60 mol/(m²·a).

The annual mean air-sea CO_2 flux varies from 0.47 to 1.45 mol/(m²·a) from 1982 to 2005. The mean CO_2 of the 24 years flux predicted by the ROMS-NPZD model is about 1.06 mol/(m²·a) averaged from the entire east of China's seas, which is equivalent to a regional total carbon of 3.22 Tg/a from the atmosphere to the ocean. However, the modeled result is smaller than the result (1.9 mol/(m²·a)) suggested by Tseng et al. (2013), but is larger than the result (0.87 mol/(m²·a)) suggested by Shim et al. (2007). Both the modeled and observed partial pressure of carbon dioxide in sea water show that the east of China's seas is a sink for the atmospheric CO_2.

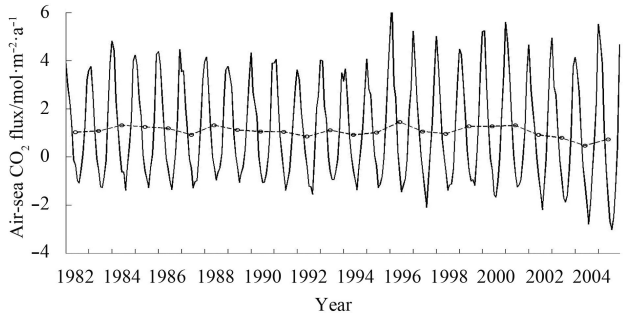

Fig. 9. Domain averaged air-sea CO_2 flux (solid line) and its annual mean value (black circle) in the east of China's seas from 1982 to 2005. The positive value is a sink, while the negative value is a source.

Figure 10 shows the interannual variation of the CO_2 flux and the Niño3 SST Index. The Niño3 SST Index measures the deviation from the normal SST in the eastern Pacific (5°S–5°N, 150°–90°W) (http://www.esrl.noaa.gov/psd/gcos_wgsp/Timeseries/Data/nino3.long.data). There is a clear inverse relationship between the Niño3 SST Index and the air-sea CO_2 flux. During the El Niño event, the CO_2 flux reduces obviously, especially in 1997. This is primarily due to the increase in the SST in the western Pacific, which results in the increase of the partial pressure of carbon dioxide in sea water in the ocean (Feely et al., 2002; Takahashi et al., 2003, 2009). Thus, the CO_2 flux in the east of China's seas is connected with the ENSO events.

4 Discussion

The partial pressure of carbon dioxide in sea water is affected by a suit of physical and biogeochemical processes including SST variations, vertical mixing, photosynthesis/respiration, calcium carbonate precipitation/dissolution, and the air-sea CO_2 exchanges. In this section, the variations of the partial pressure of carbon dioxide in sea water and pH in the east of China's seas under anthropogenic influence are discussed. The interannual variations of the partial pressure of carbon dioxide in sea water, the SST and the Chl *a* concentration on the surface are analyzed. Meanwhile, the relative effects of different factors and processes on the variability of the partial pressure of carbon dioxide in sea water on different time scales are analyzed.

4.1 *Partial pressure of carbon dioxide in sea waterand pH variation in the east of China's seas*

After removing the seasonal variation, the long-term time-series of the partial pressure of carbon dioxide in sea water and pH in the east of China's seas show pronounced interannual variations over time from 1982 to 2005 (Fig. 11). As shown in Fig. 11, the time series of the p_{CO_2sea} anomaly ranges from –20 to 60 μatm, and Chai et al. (2009) estimated that the anomaly partial pres-

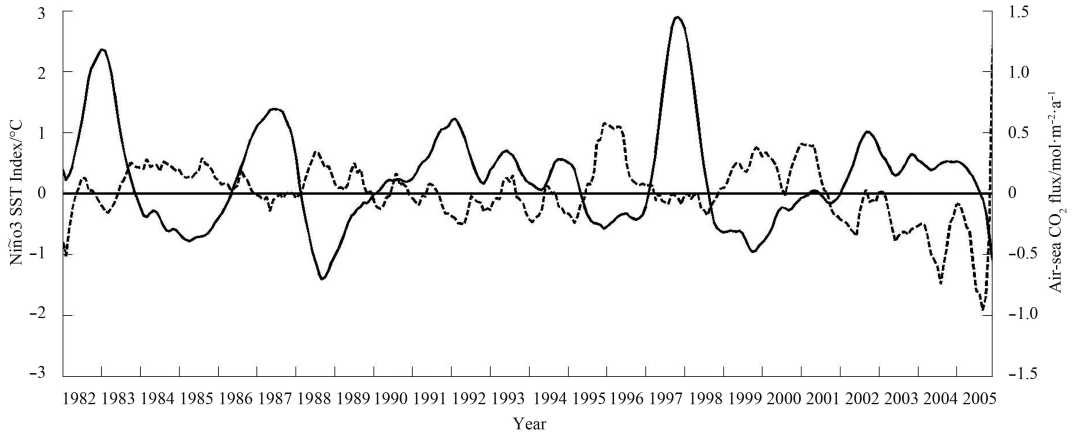

Fig. 10. Domain averaged annual mean value of air-sea CO_2 flux (black dash line) and Niño3 SST Index (black solid line) in the east of China's seas from 1982 to 2005.

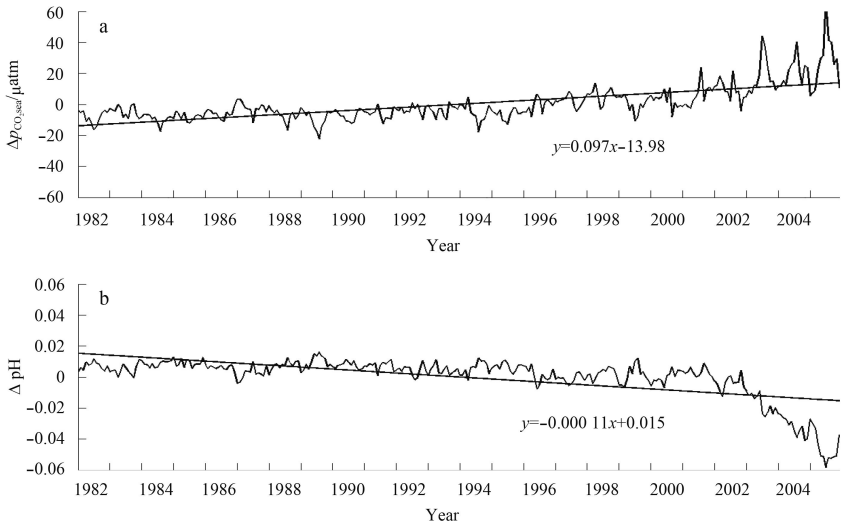

Fig. 11. For the period of 1982–2005, monthly averaged surface anomaly of p_{CO_2air} (a) and pH (b) in the east of China's seas.

sure of carbon dioxide in sea water in SCS is from –25 to 30 μatm. The partial pressure of carbon dioxide in sea water in the east of China's seas from the linear regression slopes is 1.15 μatm/a, while the estimated increasing rate in north Pacific is between 0.5 and 2.0 μatm/a, and is estimated at (1.3±0.6) μatm/a in the center and west Pacific Ocean (Takahashi et al., 2009). Hence, modeled increasing rates of the partial pressure of carbon dioxide in sea water are within the range of others' variability. Meanwhile, the p_{CO_2air} is increasing at a rate of 1.5 μatm/a in the central equatorial and subtropical northern Pacific Ocean due to anthropogenic emissions (Takahashi et al., 2003); the partial pressure of carbon dioxide in air of the east of China's seas waters follows a consistent rate of increase, which leads to the increase of acidity in the sea. The growth rates of the partial pressure of carbon dioxide in sea water and partial pressure of carbon dioxide in air agree well with each other indicating the uptake of anthropogenic CO_2 as the major cause for long-term increases in DIC and decreases in $CaCO_3$ saturation state.

The year-to-year variation of pH is in a range of –0.06–0.02, and the reducing rate is 0.001 3 a^{-1} which reveals the ocean acidification characteristic. According to the observation data, the averaged ocean surface water pH has fallen from approximately 8.21 to 8.10 by approximately 0.1 units since preindustrial times (IPCC, 2000), and is expected to decrease a further 0.3–0.4 pH units (Orr et al., 2005) if atmospheric CO_2 concentration reaches 800 μatm. Solomon (2007) also estimates the reducing rate is 0.002 a^{-1} for pH in the North Atlantic seas. The modeled pH decreasing rate is smaller than others. This discrepancy could be resulted from the fact that the time series observational data are obtained from a long-term observation in the Atlantic sea, while the modeled time is much shorter in the east of China's seas.

4.2 *Sensitivity factors of controlling partial pressure of carbon dioxide in sea water*

Surface variables (the partial pressure of carbon dioxide in sea water, the SST and the Chl *a* concentration) are examined to the seasonal variation over the entire east of China's seas (Fig. 12). Domain-averaged monthly partial pressure of carbon dioxide in sea water varies between 280 and 430 μatm with the highest value in August and the lowest value in January. According to the value of p_{CO_2air} 373 μatm, averaged from 1990 to 2004 (Chai et al., 2009), hence the east of China's seas is a sink of CO_2 to the atmosphere in winter, early spring and later autumn, and a source in the other times of the year.

In the east of China's seas the domain-averaged monthly SST is in a range of 14–28°C. The SST has the same variation tendency with the partial pressure of carbon dioxide in sea water, which reaches the highest value of 28°C in August and the lowest value of 14°C in January. As the trend line shown in Fig. 12a, the partial pressure of carbon dioxide in sea water has a positive cor-

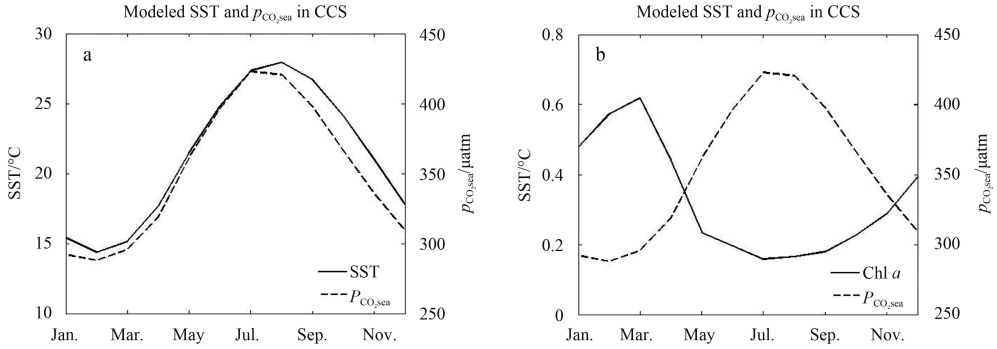

Fig. 12. Domain averaged climatologic seasonal variations of the SST (solid line) and p_{CO_2air} (dash line) (a), and the partial pressure of carbon dioxide in sea water (solid line) and Chl *a* concentration (dash line) (b) from 1982 to 2005 in the east of China's seas.

relation with the SST, which means the seasonal variation of p_{CO_2sea} is controlled by the SST.

The range of Chl *a* concentration is from 0.1 to 0.7 mg/m^3 with the highest value of 0.7 mg/m^3 in March and the lowest value of 0.1 mg/m^3 in August (Fig. 12b). Owing to the strong light intensity, warm sea water and plenty of nutrients accumulated in winter, the phytoplankton reproduces rapidly in most areas of the China's seas. It also can be found that the seasonal variation of Chl *a* concentration has an opposite tendency with the partial pressure of carbon dioxide in sea water, which means phytoplankton is another control factor of the partial pressure of carbon dioxide in sea water. During the growth of phytoplankton, CO_3^{2-} would be consumed by biological activity as a kind of nutrients; hence the partial pressure of carbon dioxide in sea water is lower in this process (Jin and Shi, 2001; Liu et al., 2002; Chai et al., 2009).

The in-phase relationship between the partial pressure of carbon dioxide in sea water and the SST and out-of-phase relationship between the partial pressure of carbon dioxide in sea water and Chl *a* concentration suggest that the partial pressure of carbon dioxide in sea water is regulated by both the SST and the biological activity in the east of China's seas.

It has been estimated that the oceanic uptake and release of CO_2 are governed by the dynamic equilibrium of the sea temperature, the biological utilization of CO_2, and the upwelling flux of subsurface waters with high CO_2 concentration (Feely et al., 2001; Takahashi et al., 2002). In order to isolate the effect of each factor on the partial pressure of carbon dioxide in sea water in the east of China's seas, a series of sensitivity experiments on basin-wide SST, SSS, TIC, and TA are conducted; one factor is set as a constant each time and assigned with its annual mean value. The standard experiment is based on the seasonal cycle of the monthly averaged SST, SSS, TIC and TA in the east of China's seas.

As shown in Fig. 13, the seasonal variation of the partial pressure of carbon dioxide in sea water varies from 280 to 430 μatm in the standard experiment, which is low in winter and high in summer. When the SST value is fixed as annual mean, the partial pressure of carbon dioxide in sea water has a pronounced change compared with the standard value. Since the annual mean value of the SST is higher in winter and lower in summer than that in the standard experiment, the seasonal amplitude of the partial pressure of carbon dioxide in sea water is from 310 to 390 μatm, and is higher in winter and lower in summer. Obviously, the seasonal cycle of the partial pressure of carbon dioxide in sea water responds to the SST changes, which also means that the SST has a strong effect on the partial pressure of carbon dioxide in sea water. When fixed the SSS and TA, both the tendency and value of the partial pressure of carbon dioxide in sea water have little changes compared with the value in the standard experiment, which means that the SSS and TA have less influence on the partial pressure of carbon dioxide in sea water. With fixed TIC, the partial pressure of carbon dioxide in the sea water has the same changing trend with that in the standard experiment, but the value has a large variation which ranges from 250 to 480 μatm. Hence, TIC has a strong effect on the partial pressure of carbon dioxide in sea water in the east of China's seas.

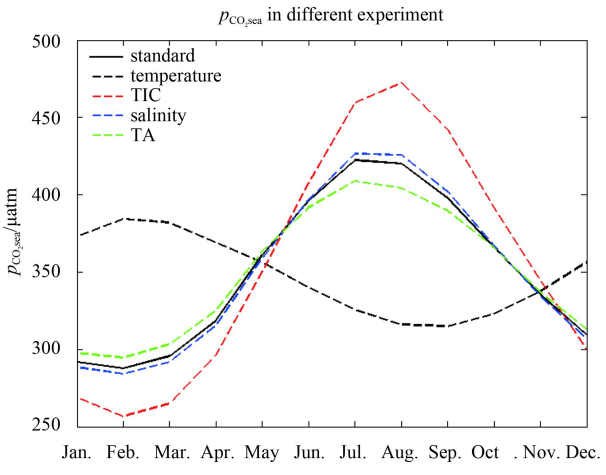

Fig. 13. The the partial pressure of carbon dioxide in sea water sensitivity experiments in the east of China's seas.

The amplitudes of the partial pressure of carbon dioxide in sea water annual variation ($\Delta p_{CO_2sea}=p_{CO_2sea,\,max}=-p_{CO_2sea,\,min}$ are 134 μatm for the standard experiment, and 69, 142, 114 and 215 μatm in the experiments with annual mean of SST, SSS, TA and TIC, respectively. The amplitude of the increment of Δp_{CO_2sea} decreases by 65 μatm under the condition of fixed SST, but it increases by 81 μatm when the TIC is set as its annual mean value. It is only a slightly change in values of 8 and 20 μatm when fixed SSS and TA.

In order to analyze the main control factor of the partial pressure of carbon dioxide in sea water in the east of China's seas, the method given by Takahashi et al. (2002) is used. The formulation is as follows: $T/B=\Delta p_T(CO_2)/\Delta p_B(CO_2)$, $T\text{-}B=\Delta p_T\text{-}(CO_2)\text{-}\Delta p_B(CO_2)$, where T refers to the temperature effect on the partial pressure of carbon dioxide in sea water, and B is the biological activity effect, hence, the relative rate of the temperature effect to the biological carbon utilization is T/B=65/81=0.80, and $T\text{-}B$=–16 μatm. Therefore, the influence of biological activity is greater than that of temperature in the east of China's seas, which is consistent with the conclusion in the north of 40°N in the northern Pacific estimated by Takahashi et al. (2002). Gypens et al. (2004) also pointed out that biological activity has stronger influence on the partial pressure of carbon dioxide in sea water than the SST in the southern bight of the North Sea.

5 Conclusions

Using a 3-D physical-biogeochemical model (ROMS-NPZD), the seasonal and inter-annual variation of the air-sea CO_2 flux in the east of China's seas and the associated control factors are evaluated. Forced by the high-frequency of the air-sea fluxes, the model is capable of reproducing the observed NO_3, TA, and DO feature in the ECS. The ROMS-NPZD simulation shows strong seasonal variations as well as interannual variations of the partial pressure of carbon dioxide in sea water and the air-sea CO_2 flux. The modeled results suggest that the east of China's seas is a CO_2 sink to the atmosphere in winter and a source in summer. The annual mean air-sea CO_2 flux shows that the east of China's seas is a sink of CO_2 to the air by 1.06 mol/(m^2·a) (3.22 Mt/a).

We conducted a sensitivity analysis to investigate the controlling mechanisms (SST, TIC, SSS, TA) of the seasonal cycle of the partial pressure of carbon dioxide in sea water. The variability of the partial pressure of carbon dioxide in sea water was controlled by the biological activity, the role of the SST and upwelling in regulating the partial pressure of carbon dioxide in sea water was secondary in the east of China's seas. From 1982 to 2005, the partial pressure of carbon dioxide in sea water increases at a rate of 1.15 μatm/a, and water pH decreases with a

rate of 0.001 3 a^{-1}, which means the east of China's seas has a prominent acidification phenomenon. The modeled results also show significant correlations of the partial pressure of carbon dioxide in sea water and the air-sea CO_2 flux in the east of China's seas with ENSO events, attributed to a strong influence of the ENSO on the SST and wind speed.

The ROMS-NPZD model simulations clearly illustrate the role of physical and biological factors in regulating the partial pressure of carbon dioxide in sea water and the air-sea CO_2 flux in the east of China's seas. This study demonstrates the need for monitoring important variables in the east of China's seas, and uses these observations for constructing and evaluating the physical and biogeochemical models. By combining both observations and model simulations, we can advance our understanding on the global carbon cycle and climate change.

Acknowledgements

The authors appreciate the help provided by Qiao Ran and Lyu Honggang for the observation data.

References

Blumberg A F, Kantha L H. 1985. Open boundary conditions for circulation models. J Hydr Engin, 111(2): 237–255

Bozec Y, Thomas H, Elkalay K, et al. 2005. The continental shelf pump for CO_2 in the North Sea-Evidence from summer observation. Marine Chemistry, 93(2–4): 131–147

Cai Weijun, Dai Minhan, Wang Yongchen. 2006. Air-sea exchange of carbon dioxide in ocean margins: a province-based synthesis. Geophysical Research Letters, 33(12): L12603, doi: 10.1029/2006GL026219

Chai Fei, Liu Guimei, Xue Huijie, et al. 2009. Seasonal and interannual variability of carbon cycle in South China Sea: a three-dimensional physical-biogeochemical modeling study. Journal of Oceanography, 65(5): 703–720

Duan Shuiwang, Zhang Shen. 1999. The variations of nitrogen and phosphorus concentrations in the monitoring stations of the three major rivers in China. Scientia Geographica Sinica (in Chinese), 19(5): 411–416

Feely R A, Boutin J, Cosca C E, et al. 2002. Seasonal and interannual variability of CO_2 in the equatorial Pacific. Deep Sea Research Part II: Topical Studies in Oceanography, 49(13–14): 2443–2469

Feely R A, Sabine C L, Takahashi T, et al. 2001. Uptake and storage of carbon dioxide in the ocean: The global CO_2 survey. Oceanography, 14(4): 18–32

Fennel K, Wilkin J, Levin J, et al. 2006. Nitrogen cycling in the middle Atlantic bight: results from a three-dimensional model and implications for the North Atlantic nitrogen budget. Global Biogeochemical Cycles, 20(3): GB3007, doi: 10.1029/2005GB002456

Gruber N, Frenzel H, Doney S C, et al. 2006. Eddy-Resolving Simulation of Plankton Ecosystem Dynamics in the California Current System. Deep Sea Research Part Ⅰ: Oceanographic Research Papers, 53(9): 1483–1516

Gypens N, Lancelot C, Borges A V. 2004. Carbon dynamics and CO2 air-sea exchanges in the eutrophied coastal waters of the southern bight of the North Sea: a modeling study. Biogeosciences Discussions, 1: 561–589

Hu Haoguo, Wan Zhenwen, Yuan Yeli. 2004. Simulation of seasonal variation of phytoplankton in the southern Huanghai (Yellow) Sea and analysis on its influential factors. Haiyang Xuebao (in Chinese), 26(6): 74–88

Ji Xuanliang, Liu Guimei, Gao Shan, et al. 2015. Parameter sensitivity study of the biogeochemical model in the china coastal seas. Acta Oceanologica Sinica, 34(12): 51–60, doi: 10.1007/s13131–015-0762–0

Jin Xin, Shi Guangyu. 2001. The role of biological pump in ocean carbon cycle. Chinese Journal of Atmospheric Sciences (in Chinese), 25(5): 683–688

Large W G, McWilliams J C, Doney S C. 1994. Oceanic vertical mixing: a review and a model with a nonlocal boundary layer parameterization. Reviews of Geophysics, 32(4): 363–403

Liu Hao, Yin Baoshu. 2007. Model study on Bohai ecosystem: II. Annual cycle of nutrient-phytoplankton dynamics. Haiyang Xuebao (in Chinese), 29(4): 20–33

Liu K K, Chao S Y, Shaw P T, et al. 2002. Monsoon-forced chlorophyll distribution and primary production in the south china sea: observations and a numerical study. Deep Sea Research: Part I. Oceanographic Research Papers, 49(8): 1387–1412

Lu Zhongming, Gan Jianping, Dai Minhan. 2012. Modeling seasonal and diurnal pCO_2 variations in the northern South China Sea. Journal of Marine Systems, 92(1): 30–41

Millero F J. 1995. Thermodynamics of the carbon dioxide system in the oceans. Geochimica et Cosmochimica Acta, 59(4): 661–677

Morel A, Berthon J F. 1989. Surface pigments, algal biomass profiles, and potential production of the euphotic layer: relationships reinvestigated in view of remote-sensing applications. Limnology and Oceanography, 34(8): 1545–1562

Naqvi S W A, Bange H W, Gibb S W, et al. 2005. Biogeochemical ocean-atmosphere transfers in the Arabian Sea. Progress in Oceanography, 65(2–4): 116–144

Orr J C, Fabry V J, Aumont O, et al. 2005. Anthropogenic ocean acidification over the twenty-first century and its impact on calcifying organisms. Nature, 437(7059): 681–686

Qiao Ran, Wang Zhanggui, Zhang Bing, et al. 2005. Observation and research of carbon dioxide in the ocean. Marine Forecasts (in Chinese), 22(S1): 106–114

IPCC. 2000. Special Report on Emission Scenarios. A special Report of Working Group III of the Intergovernmental Panel on Climate Change. Cambridge: Cambridge University Press

Shchepetkin A F, McWilliams J C. 2003. A method for computing horizontal pressure-gradient force in an oceanic model with a nonaligned vertical coordinate. Journal of Geophysical Research: Ocean, 108(C3): 3090

Shim J, Kim D, Kang Y C, et al. 2007. Seasonal variations in pCO_2 and its controlling factors in surface seawater of the northern East China Sea. Continental Shelf Research, 27(20): 2623–2636

Solomon S, Qin D, Manning M, et al. 2007. Climate change 2007: Synthesis Report. Contribution of Working Group I, II and III to the Fourth Assessment Report of the Intergovernmental Panel on Climate Change. Summary for Policymakers. Cambridge: Cambridge University Press

Takahashi T, Sutherland S C, Feely R A, et al. 2003. Decadal variation of the surface water pCO_2 in the western and central equatorial Pacific. Science, 302(5646): 852–856

Takahashi T, Sutherland S C, Sweeney C, et al. 2002. Global sea-air CO_2 flux based on climatological surface ocean pCO_2, and seasonal biological and temperature effects. Deep Sea Research: Part II. Topical Studies in Oceanography, 49(9–10): 1601–1622

Takahashi T, Sutherland S C, Wanninkhof R, et al. 2009. Climatological mean and decadal change in surface ocean pCO_2, and net sea-air CO_2 flux over the global oceans. Deep Sea Research: Part II. Topical Studies in Oceanography, 56(8–10): 554–577

Tseng C M, Liu K K, Gong G C M, et al. 2011. CO_2 uptake in the East China Sea relying on Changjiang runoff is prone to change. Geophysical Research Letters, 38(24): L24609, doi: 10.1029/2011GL049774

Tseng C M, Shen P Y, Liu K K. 2013. Synthesis of observed air-sea CO_2 exchange fluxes in the river-dominated East China Sea and improved estimates of annual and seasonal net mean fluxes. Biogeosciences Discussions, 10(8): 13977–14007, doi: 10.5194/bgd-10–13977-2013

Tsunogai S, Watanabe S, Nakamura J, et al. 1997. A preliminary study of carbon system in the East China Sea. Journal of Oceanography, 53(1): 9–17

Tsunogai S, Watanabe S, Sato T. 1999. Is there a "continental shelf pump" for the absorption of atmospheric CO_2?. Tellus B, 51(3): 701–712

Wang Menghua, Shi Wei. 2005. Estimation of ocean contribution at the MODIS near-infrared wavelengths along the east coast of

the U.S.: two case studies. Geophysical Research Letters, 32(13): L13606

Wang Menghua, Tang Junwu, Shi Wei. 2007. MODIS-derived ocean color products along the China East coastal region. Geophysical Research Letters, 34(6): L06611

Wang S L, Chen C T A, Hong G H, et al. 2000. Carbon dioxide and related parameters in the East China Sea. Continental Shelf Research, 20: 525–544

Wang Xiujun, Christian J R, Murtugudde R, et al. 2006. Spatial and temporal variability of the surface water pCO_2 and air-sea CO_2 flux in the equatorial Pacific during 1980–2003: a basin-scale carbon cycle model. Journal of Geophysical Research: Oceans, 111(C7): C07S04

Wanninkhof R. 1992. Relationship between wind speed and gas exchange over the ocean. Journal of Geophysical Research, 97(C5): 7373–7382

Weiss R F, Price B A. 1980. Nitrous oxide solubility in water and seawater. Marine Chemistry, 8(4): 347–359

Xue Liang, Zhang Longjun, Cai Weijun, et al. 2011. Air-sea CO_2 fluxes in the southern Yellow Sea: an examination of the continental shelf pump hypothesis. Continental Shelf Research, 31(18): 1904–1914

Zhang Jing. 1996. Nutrient elements in large Chinese estuaries. Continental Shelf Research, 16(8): 1023–1045

Zhang Longjun, Zhang Yun. 2008. The distribution of partial pressure of CO_2 in the Bohai Sea in summer. Periodical of Ocean University of China (in Chinese), 38(4): 635–639

Zhang Xiaoxiao, Yao Qingzheng, Chen Hongtao, et al. 2010. Seasonal variation and fluxes of nutrients in the lower reaches of the Yellow River. Periodical of Ocean University of China (in Chinese), 40(7): 82–88

Zheng Xiaoshen, Wei Hao, Wang Yuheng. 2012. Seasonal and interannual variations of Chl a concentration based on the remote sensing data in the yellow sea and East China Sea. Oceanologia et Limnologia Sinica (in Chinese), 43(3): 649–654